Examples of application of beam propagation method for solving dynamic diffraction problems in crystals: Laue geometry, asymmetric reflections, bend crystals, and dislocations

Jacek Krzywinski[a] and Aliaksei Halavanau[a]

[a]SLAC National Accelerator Laboratory, 2575 Sand Hill Road , Menlo Park CA 94025, USA

ABSTRACT

We will present examples of using a fast Fourier transforms Beam Propagation Method (FFT BPM) to solve different dynamical diffraction problems in crystals. We will describe simulations for asymmetric reflections, in the Laue geometry and for bend crystals. The results of the FFT BPM simulations for bend crystals are in are in the perfect agreement with numerical solutions of the Takagi–Taupin equations for bend crystals reported in the literature. We will support each case by showing its numerical implementation in a Python code from a public GitHub repository. The numerical code is structured in such a way that is convenient for parallel computing.

Keywords: dynamical diffraction; Fourier optics; beam propagation method.

1. INTRODUCTION

Recently, we developed a new approach for solving time-dependent dynamic diffraction problems in distorted crystals using the Fast Fourier Transform Beam Propagation Method (FFT BPM). Our publication on this topic[1] focused on describing the theoretical approach and included several examples in the Bragg geometry. Here, we provide a more detailed description of the numerical implementation of our theory in Python. This implementation is optimized for parallel computing, and the Python code is available in a public GitHub repository.[2] We will also present simulation examples for asymmetric reflections, Laue geometry, bent crystals, and crystals with dislocations. The examples involving bent crystals and crystals with dislocations illustrate how to account for non-uniform strain distribution inside the crystal when simulating dynamic diffraction using the FFT BPM method. We also used these cases to compare FFT BPM simulations with numerical solutions of the Takagi–Taupin equations for distorted crystals reported in the literature. For continuity, we will repeat some sections of our previous paper to maintain the reading flow

2. THEORETICAL APPROACH

The scalar Helmholtz equation for a constant angular frequency ω:

$$\left(\nabla^2 + k(n(x,y,z))^2\right) E(x,y,z) = 0 \tag{1}$$

can be written in the following form:[3,4]

$$\frac{d\psi}{d\hat{z}} = i\left(\sqrt{1+{\nabla_\perp}^2 - \delta\epsilon(\hat{x},\hat{y},\hat{z})} - 1\right)\psi \tag{2}$$

where $\hat{x},\hat{y},\hat{z} = kx, ky, kz$, k is the wave vector,${\nabla_\perp}^2$ is the Laplace operator taken with respect to the transverse coordinates $\hat{x},\hat{y}$, $\delta\epsilon(\hat{x},\hat{y},\hat{z}) = n(\hat{x},\hat{y},\hat{z})^2 - \bar{n}^2$, $n(\hat{x},\hat{y},\hat{z})$ is the refractive index, $\bar{n}$ is its average value and

Further author information: (Send correspondence to J. Krzywinski)
J. Krzywinski.: E-mail: krzywins@slac.stanford.edu,
A. Halavanau: E-mail: aliaksei@slac.stanford.edu

$E(x,y,z) = \psi(x,y,z)e^{-ikz}$. In the case of beams with narrow angular spectrum this equation can be approximated by:

$$\frac{d\psi}{d\hat{z}} = i\left(\sqrt{1+{\nabla_\perp}^2} - \frac{\delta\epsilon(\hat{x},\hat{y},\hat{z})}{2\sqrt{1-\left\langle k_x^2+k_y^2\right\rangle}} - 1\right)\psi \tag{3}$$

Here the operator $\sqrt{1+{\nabla_\perp}^2}$ in the denominator of the second term of the r.h.s was approximated by $\sqrt{1-\left\langle k_x^2+k_y^2\right\rangle}$ where $\left\langle k_x^2+k_y^2\right\rangle$ is the average angular spectrum and $k_x^2+k_y^2 = F[{\nabla_\perp}^2]$ is the Fourier transform of the ${\nabla_\perp}^2$ operator. Eq. (3) leads to the following FFT BPM equation:

$$\psi(\hat{x},\hat{y},\hat{z}+\Delta\hat{z}) \approx F^{-1}\left\{F\left[\psi(\hat{x},\hat{y},\hat{z})\right]e^{i\Delta\hat{z}\sqrt{1-k_x^2-k_y^2}}\right\}e^{i\Delta\hat{z}\frac{\delta\epsilon(\hat{x},\hat{y},\hat{z})}{2\cos\alpha}} \tag{4}$$

where F and F^{-1} denote Fourier and inverse Fourier transforms, $\cos\alpha = \sqrt{1-\left\langle k_x^2+k_y^2\right\rangle}$. The angle α corresponds to the grazing incidence angle with respect to the propagation direction. We have previously applied Eq. (4) to take into account dynamic diffraction effects when simulating interaction of x-ray beams with gratings and multilayer optics.[5–8]

In a large class of dynamical diffraction problems, the angular spectrum of the scattered x-ray beams consists of two narrow bands centered around the incident and the reflection angles. The meaningful information is contained within these bands. One can remove the fast oscillating component related to inter-planar spacing from the physical picture and derive FFT BPM equations for slowly varying envelopes of transmitted and reflected beams. For simplicity, we are considering the 2D (x,z) case, and the generalization to the 3D case is straightforward. The procedure is outlined below. First, one can write the scattered x-ray field as a sum of two components:

$$\psi(\hat{z},\hat{x}) = \psi(\hat{z},\hat{x})_+ + \psi(\hat{z},\hat{x})_-. \tag{5}$$

Then the slowly varying envelopes are defined as follows:

$$\widetilde{\psi}(\hat{z},\hat{x})_+ = \psi(\hat{z},\hat{x})_+ e^{-i\frac{k_d}{2}\hat{x}}, \quad \widetilde{\psi}(\hat{z},\hat{x})_- = \psi(\hat{z},\hat{x})_- e^{i\frac{k_d}{2}\hat{x}} \tag{6}$$

where k_d is the reciprocal vector related to inter-planar spacing. Next we expand the exponential term related to dielectric susceptibility in Eq. (4) as:

$$e^{i\hat{z}\frac{\delta\epsilon(\hat{z},\hat{x})}{2cos\alpha}} = \sum_{n=-\infty}^{+\infty}\Delta\epsilon(\hat{z},\hat{x})_n e^{ik_d n\hat{x}} \tag{7}$$

We treat deformation of the crystal as modification of the susceptibility:[9]

$$\Delta\epsilon_n^{'}(\hat{z},\hat{x}) = \Delta\epsilon_n(\hat{z},\hat{x})e^{in\mathbf{k_d}\mathbf{u}(\hat{z},\hat{x})} \tag{8}$$

where $\mathbf{k_d}\mathbf{u}$ is a scalar product of the reciprocal and displacement vectors. We note that $\mathbf{k_d}$ is parallel to $\hat{x}$ by definition, therefore only x-component of $\mathbf{k_d}$ is used.

It has been shown in our previous paper[1] that one arrives at the following set of equations for slowly varying envelopes $\widetilde{\psi}(\hat{z},\hat{x})_+$ and $\widetilde{\psi}(\hat{z},\hat{x})_-$:

$$\begin{aligned}\widetilde{\psi}(\hat{z}+\Delta\hat{z},\hat{x})_+ &= \widetilde{\psi}(\hat{z},\hat{x})_{p+}\Delta\epsilon_0(\hat{z},\hat{x}) + \widetilde{\psi}(\hat{z},\hat{x})_{p-}\Delta\epsilon_{+1}^{'}(\hat{z},\hat{x})\\ \widetilde{\psi}(\hat{z}+\Delta\hat{z},\hat{x})_- &= \widetilde{\psi}(\hat{z},\hat{x})_{p-}\Delta\epsilon_0(\hat{z},\hat{x}) + \widetilde{\psi}(\hat{z},\hat{x})_{p+}\Delta\epsilon_{-1}^{'}(\hat{z},\hat{x}),\end{aligned} \tag{9}$$

where $\widetilde{\psi}(\hat{z},\hat{x})_{p\pm} = F^{-1}\left[F\left[\widetilde{\psi}(\hat{z},\hat{x})_\pm\right]p_\mp\right]$. The operators $p_\pm = e^{i\Delta\hat{z}\sqrt{1-(k_x\pm\frac{k_d}{2})^2}}$ correspond to the Fourier image of ${\nabla_\perp}^2$ which is shifted by $\pm\frac{k_d}{2}$ in the angular spectrum space. Equation (4) can be rewritten in the operator

form as:

$$\begin{aligned}\psi(\hat{x},\hat{y},\hat{z}+\Delta\hat{z}) &\approx \prod_i A(a_i\Delta_z)B(b_i\Delta_z)\psi(\hat{x},\hat{y},\hat{z}), \\ A &= F^{-1}\left\{F\left[\psi(\hat{x},\hat{y},\hat{z})\right]e^{ia_i\Delta\hat{z}\sqrt{1-k_x^2-k_y^2}}\right\}, \\ B &= e^{ib_i\Delta\hat{z}\frac{\delta\epsilon(\hat{x},\hat{y},\hat{z})}{2\cos\alpha}}.\end{aligned} \tag{10}$$

In the case of first order splitting, when $a_1 = 1, b_1 = 1$, Eq. (10) is reduced to Eq. (4). For most of the practical problems this splitting scheme is accurate. Higher order splitting improves the efficiency of the FFT BPM for large Bragg angles. For instance, when $a_1 = 0.0, a_2 = 1.0, b_1 = 0.5, b_2 = 0.5$, Eq. (10) is accurate up to $O(\Delta z^2)$, and when $t = 1.3512, a_1 = 0.0, a_2 = t, a_3 = 1-2t, a_4 = t, b_1 = t/2, b_2 = (1-t)/2, b_3 = (1-t)/2, b_4 = t/2$ it is accurate up to $O(\Delta z^4)$; see.[10]

.

We point out that Eqs. (9) can be treated as a two-beam approximation for the FFT BPM. These equations are analogous to the Takagi-Taupin equations (TTE) in two-beam approximation.[9] However, there is a significant difference between TTE and FFT BPM equations. The TTE equations are a system of hyperbolic equations where the second derivatives in the transverse direction with respect to beam propagation are neglected. Therefore, diffraction of the x-rays is not taken into account in the TTE formulation. The numerical algorithms for solving TTE, which are presented in the literature, typically require setting the boundary conditions. This could be a difficult problem itself in complicated geometries or when the boundaries are not very well defined. On the other hand, the FFT BPM equations are a system of parabolic equations that automatically includes diffraction. Also, as we have mentioned before, the FFT BPM method is especially convenient when dealing with complicated shapes or non-homogeneous boundaries.

3. NUMERICAL IMPLEMENTATION

The algorithm is embedded in a class; the user provides configuration file (in yaml format) to run a simulation instance, for example for a given angle of incidence and/or wavelength. Since most of the diffraction problems are "linear", all instances, in principle, can be evaluated in parallel. The input configuration file provides the main input simulation parameters and data: photon energy, crystallographic data, electric susceptibilities, crystal geometry, numerical grid parameters, integration methods and parameters, x-ray beam properties, crystal deformation data and program settings. The user interacts with the code using jupyter notebooks or user scripts (similar to SRW approach). Python scripts are grouped in three classes:[2] XBPM, XCrystal and XCrTools

The main propagation equations, Eqs. (9-14) from our previous paper,[1] are encoded in the XBPM class. The XCrTools class is used to configure the incident x-ray beam and to provide numerical tools needed for manipulations such as FFT, padding, cropping, interpolation, etc. The XCrystal class incorporates the parameters and data provided in the yaml configuration file and creates the main 'run3D()' function. The 'run3D()' can be used to define a single realization reflection object that is computed in parallel to other reflections having different parameters e.g. photon energy, incidence angle, etc. Thus, the calculation of rocking curves or time-dependent diffraction can be implemented as an embarrassingly parallel problem.

4. SIMULATION OF REFLECTION IN THE LAUE GEOMETRY AND ASYMMETRIC REFLECTIONS

Previously we have shown simulations of the symmetric Bragg reflection cases. Now let us consider the Laue geometry and the diamond crystal for (400) reflection at 9.831 keV photon energy. The crystal has a form of a slab. Let us define the s-axis to be perpendicular to the crystal's surfaces. The orientation of the s-axis with respect to the crystallographic planes is defined by the *asymm_angle* parameter in the configuration yaml file. The Bragg geometry corresponds to $asymm\_angle = 0\ deg$ and the Laue geometry corresponds to the $asymm\_angle = 90\ deg$.

An example of a simulation of reflection in the Laue geometry is implemented in the `SingleRealization_C400_Laue.ipynb` Jupyter notebook, which can be found in the example directory of the Crystal-fft-bpm GitHub repository.[2] The corresponding configuration file, `C400_9p8keV_LaueFig1.yaml`, is located in the config directory. Results of the simulation are presented in Fig. 1. Two cases are simulated: when the incident beam is at the Bragg angle (top left) and at the Bragg angle + 1.5 μrad (top right).

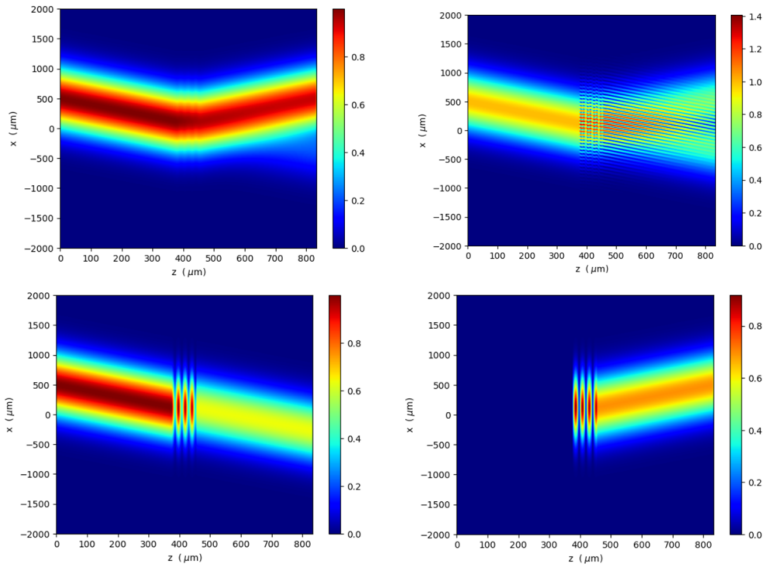

Figure 1. 2D visualization of a diamond (400) Laue reflection, with the incident beam at the Bragg angle (top left) and at the Bragg angle + 1.5 μrad (top right). The bottom row shows the intensity of the transmitted component $\widetilde{\psi}+$ (left) and the reflected part $\widetilde{\psi}-$ for the 1.5 μrad deviation from the Bragg angle. The Pendellösung oscillations are clearly visible. The color scale units are arbitrary

The asymmetric reflection geometries correspond to the situation when $0° <$ `asymm_angle` $< 90°$. The visualization of asymmetric reflection for an asymmetry angle corresponding to `asymm_angle` $= 15°, -15°$ is depicted in Fig. 2. The corresponding Jupyter notebook and configuration file for `asymm_angle` $= 15°$ are: `SingleRealization_C400_AsymetricReflection.ipynb` and `C400_9p8keV_LaueAssymRefl15degFig2.yaml`. The deviations from the Bragg for `asymm_angle` $= 15°, -15°$ were 20 μrad and 10 μrad respectively.

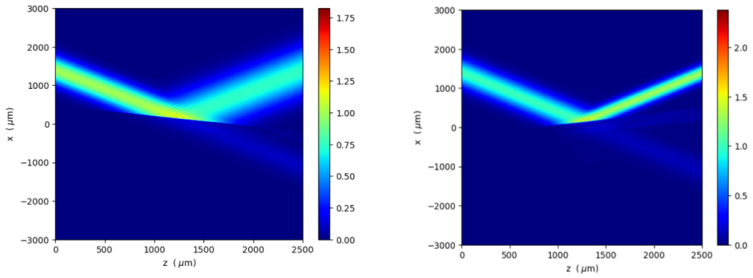

Figure 2. 2D visualization of field amplitudes for a diamond (400) asymmetric reflection, asymm_angle=15 *deg* (left), asymm_angle=15 *deg* (right). Color scale units are arbitrary.

The rocking curve for the Laue case was computed using the parallel algorithm outlined in the previous paragraph, with parallelization performed with respect to the incident angle. The results obtained using the FFT BPM method are compared to those from the XOP toolkit,[11] as shown in Fig. 3. We note excellent

agreement between our method and the XOP output. The very small differences between the two plots can be attributed to the finite beam waist and numerical errors due to the finite mesh size. The corresponding Python code for parallel computing, the Jupyter notebook for displaying the results, and the configuration file are: `run_parallel_angleC400_9831eV_Laue.py`, `process-parallel-data-angleC400_9p8keV_Laue.ipynb`, and `C400_9p8keV_LaueFig3.yaml`.

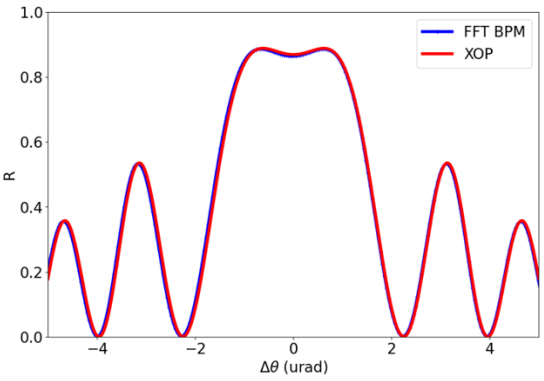

Figure 3. Rocking curve simulated in the Laue geometry for a 82 μm thick diamond crystal at 9.813 keV photon energy.

5. SIMULATIONS OF BEND CRYSTALS

Bend crystals have been successfully used to built single shot spectrometers for XFEL applications.[12,13] To benchmark our code, we simulated rocking curves for a bend diamond crystal applied at the European X-ray Free-Electron Laser. The rocking curves from this crystal were investigated theoretically in the article by L.Samoylova et al.[14] In that paper the simulations were done for a 20 μm thick crystal bent around the axis [001] (y axis) with a surface orientation [110] (z axis). The displacement u_z for cylindrically bend crystal can be expressed as:

$$u_z = \frac{1}{2R}\left(x^2 + \nu z^2\right) \tag{11}$$

where R is the bending radius and ν is the Poisson ratio.[14] The scattering from the bend crystal was derived by a numerical solution of the Takagi–Taupin equations based on the algorithm proposed by Authier et al.[9] The authors considered a symmetric Bragg reflection 440 of monochromatic x-ray at 14.4 keV. The incident wave front was restricted to a width of 10 mm by an entrance slits.

We have simulated the same case using our FFTBPM method. The rocking curves for two bending radii of R= 65 mm and R= 95 mm are presented in Fig. 4

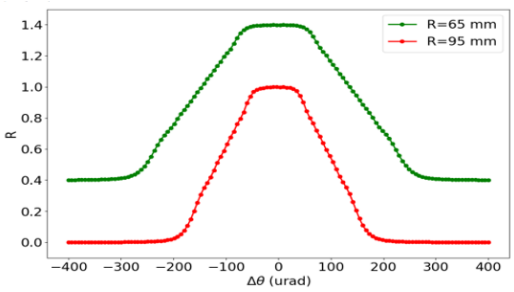

Figure 4. Rocking curves simulated for bending radii of 65 and 95 mm.

The results calculated using our FFT BPM method, presented in Fig. 4, are identical to the numerical solution of the Takagi–Taupin equations shown in Fig. 2 in the article by L.Samoylova et al..[14] The corresponding

Python code for parallel computing, the Jupyter notebook for displaying the results, and the configuration file are: `run_parallel_angleC440CurvedSpectrometer.py`, `process-parallel-data-angleC440Spectrometer.ipynb`, and `CrystalC440Fig4.yaml`

6. SIMULATIONS OF DISLOCATIONS

Our FFT BPM method can be easily applied to simulate crystal defects such as dislocations. We will simulate two cases that were investigated using TTE approach: a Laue [220] and [440] reflections from a Si crystal in the presence of screw and mixed dislocations.[9],[15],[16]

The first case follows an examples the presented in the work of I. S. Besedin et al.[15] A plane-parallel silicon plate was chosen to be a model crystal. In this structure, undissociated straight-line dislocations have a Burgers vectors, with a magnitude $|\mathbf{b}| = \mathrm{a}/\sqrt{2}$,where a is the lattice constant The burgers vectors and and the diffraction vector $\boldsymbol{h}$ are directed along the (110) axis. The photon energy We will consider two types of dislocations here: a screw dislocation, and a mixed 60 degrees dislocation. The screw dislocation has the unit dislocation line vector $\boldsymbol{\tau}$ parallel to the Burgers vector (along the(110) axis). The mixed 60 degrees dislocation has the unit dislocation line vector $\boldsymbol{\tau}$ parallel to the (101) axis as it is indicated in Fig. 5. The coordinate system (x,y,z) corresponds to (1,1,0), (-1,1,-2) and (-1,1,1) axes respectively. We consider a symmetric reflection [220] at $\lambda = 0.0709$ nm. The crystal thickness 363 μm corresponds to 10 Λ where Λ is the extinction length.

According to[15] the displacement vector u(r) for a straight-line dislocation in its intrinsic coordinate system (x_0,y_0,z_0), has the form:

$$\boldsymbol{u} = \frac{\boldsymbol{b}}{2\pi}\arctan\frac{z_0}{y_0} + \frac{\boldsymbol{b} - \boldsymbol{\tau}(\boldsymbol{b}\cdot\boldsymbol{\tau})}{2\pi}\frac{y_0 z_0}{2(1-\nu)(y_0^2+z_0^2)} - \frac{\boldsymbol{\tau}\times\boldsymbol{b}}{2\pi}\left(\frac{1-2\nu}{4(1-\nu)}\ln(y_0^2+z_0^2) + \frac{y_0^2-z_0^2}{4(1-\nu)(y_0^2+z_0^2)}\right) \quad (12)$$

where the x_0 axis is directed along $\boldsymbol{\tau}$, the z_0 axis is directed along the vector $\boldsymbol{\tau}\times\boldsymbol{b}$, and ν is the Poisson ratio ($\nu = 0.22$ for silicon).

We are only concern with the u_x component of $\boldsymbol{u}$ vector. Therefore, for the case considered here the equation (12) simplifies to:

$$u_x = \frac{a}{\sqrt{2}2\pi}\arctan\frac{z_0}{y_0} \quad (13)$$

for the screw dislocation and to

$$u_x = \frac{a}{\sqrt{2}2\pi}\left(\arctan\frac{z_0}{y_0} + \frac{y_0 z_0}{4(1-\nu)(y_0^2+z_0^2)}\right) \quad (14)$$

for the 60 degree mixed dislocation. The coordinates (x_0,y_0,z_0) are related to the coordinates (x,y,z) via the matrix transformation $\boldsymbol{M}$, where x_d, y_d and z_d are positions of the origin of intrinsic coordinate system of dislocation with respect to the origin of the coordinates (x,y,z).

$$\begin{bmatrix} x_0 \\ y_0 \\ z_0 \end{bmatrix} = \boldsymbol{M}\begin{bmatrix} x - x_d \\ y - y_d \\ z - z_d \end{bmatrix} \quad (15)$$

where $\boldsymbol{M} = \begin{bmatrix} 1 & 0 & 0 \\ 0 & -1 & 0 \\ 0 & 0 & 1 \end{bmatrix}$ for the screw dislocation case, and $\boldsymbol{M} = \begin{bmatrix} \frac{1}{2} & -\frac{\sqrt{3}}{2} & 0 \\ \frac{\sqrt{3}}{2} & -\frac{1}{2} & 0 \\ 0 & 0 & 1 \end{bmatrix}$ for the mixed 60 degrees dislocation case.

Results of XBPM simulations are presented in Fig. 6 and Fig. 7. In general, the XBPM results match those obtained by the TTE method by I. S. Besedin et al.[15] For example, the intensity distribution inside the crystal, shown on the left side of Fig. 6, coincides with the intensity presented in Fig. 4(a) of.[15] Similarly, the distribution shown on the left side of Fig. 7 agrees with the intensity pattern presented in Fig. 4(e) of.[15] We also noticed, when comparing the results, that the vertical scale of Fig. 4(e) in the work of I. S. Besedin et al. was

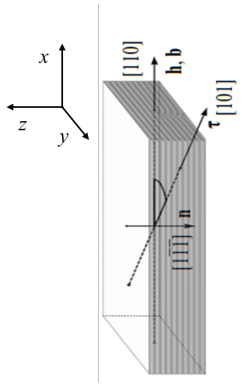

Figure 5. Geometry of the Laue [220]reflection from a Si crystal in the presence of screw and mixed dislocations. The screw dislocation has the unit dislocation line vector $\boldsymbol{\tau}$ parallel to the Burgers vector (along the(110) axis). The mixed 60 degrees dislocation has the unit dislocation line vector $\boldsymbol{\tau}$ parallel to the (101) axis. The pattern on the crystal sides indicates the Pendellösung fringes.

not consistent with the trigonal coordinate system used, requiring an increase in scale by roughly 25 %. Only after making this correction did the results obtained by XBPM and TTE agree.

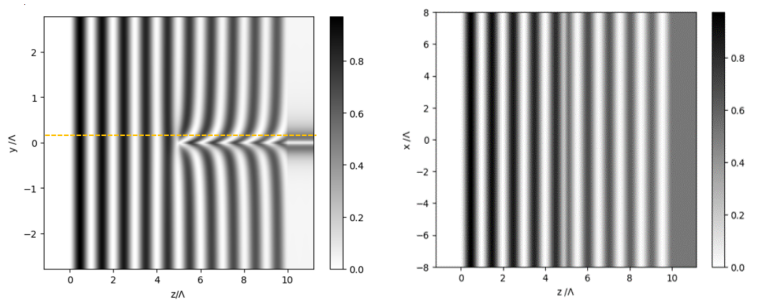

Figure 6. The intensity of the reflected wave in the Si crystal with a screw dislocation, calculated using the XBPM method, is shown in the yz (left) and xz (right) planes. The cross-section in the xy plane is taken at the position of x, indicated by the dotted line in the left figure.

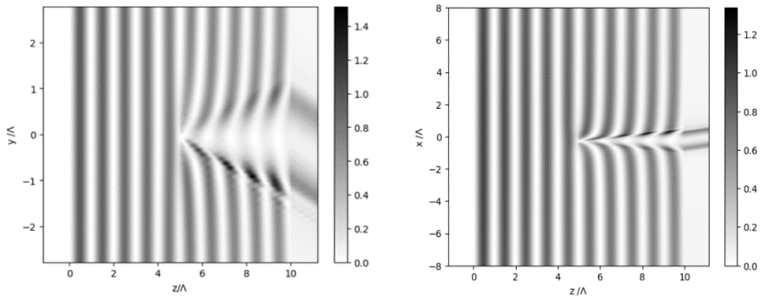

Figure 7. Intensity of the reflected wave in the Si crystal with a mixed 60 degrees dislocation.The results are identical to to the results obtained by the TTE method (Fig. 4(e) in [Chuchkovski]).

We also show in Fig. 8 the intensity of the diffracted wave in the *xy* plane after the beam exits the crystal. This corresponds to X-ray topography images taken with a monochromatic beam (Fig. 8). The corresponding Jupyter notebooks and configuration files are:

`SingleRealization_Si220_17p45keVScrewDislChukhovskii.ipynb` and `Si220_17p45keVScrewDislChukhovskii.yaml` for the screw dislocation, and `SingleRealization_60degDislocationSi220_17p45keVChukhovskii.ipynb` and `Si220_17p45keVDislChukhovskii.yaml` for the 60-degree mixed dislocation.

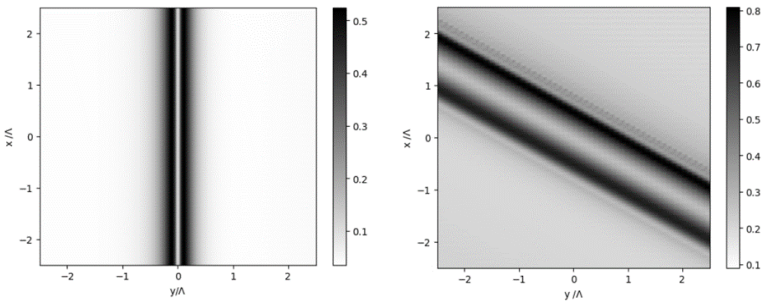

Figure 8. Intensity of the diffracted wave in the xy plane after the beam exits the crystal, left for the screw dislocation and, right for the mixed 60 degrees dislocation.

In the previous examples, the dislocation lines were parallel to the crystal's scattering surface. Now, we will present an example where the dislocation line is not parallel to the surface. We will simulate an X-ray section topography experiment as described in the paper by G. Kowalski et al.[16] The simulations were performed for the (440) and (220)reflection at 17,450 eV photon energy. A 415 µm thick [112]-oriented silicon single crystal contained a mixed 60 degrees [110] dislocation line with a 1/2 [1 -1 0] Burgers vector **b**. The geometry of the simulation is shown in Fig. 9. The transformation matrix $\boldsymbol{M}$ for this case is given by : $\boldsymbol{M} = \begin{bmatrix} 0 & -\sqrt{\frac{2}{3}} & -\sqrt{\frac{1}{3}} \\ 1 & 0 & 0 \\ 0 & \sqrt{\frac{1}{3}} & -\sqrt{\frac{2}{3}} \end{bmatrix}$. In the X-ray section topography method, the incoming X-ray beam is shaped by a slit with a width on the order of micrometers. I our case we have applied 5 μm wide slit.

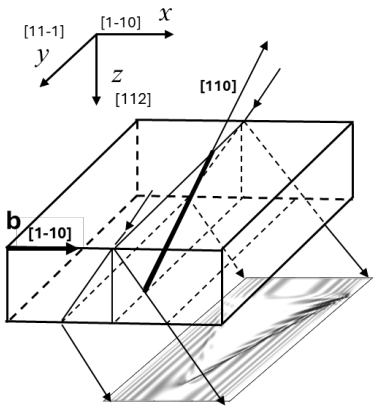

Figure 9. The geometry of the simulation.

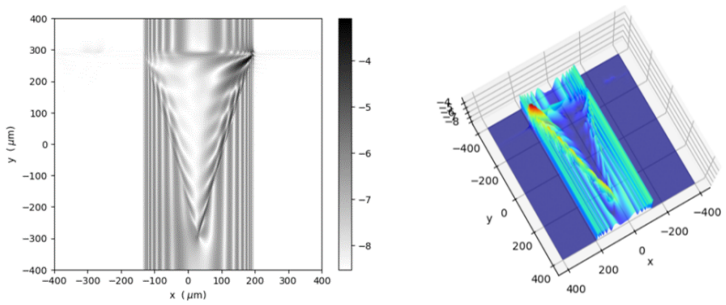

Figure 10. Simulation of a topography of a mixed 60 deg dislocation in a Si crystal by the Lang method for (220) reflection. The intensity scale is logarithmic

The results of the simulations, presented in Fig. 10 and Fig. 11, are in qualitative agreement with those presented in the work of G. Kowalski et al.[16] Unfortunately, we were unable to make a quantitative comparison, as the authors of the cited work did not provide sufficient information regarding intensity scaling in the presented figures.

The corresponding Jupyter notebooks and configuration files are:

`SingleRealization_Si220_17p45keVScrewDislChukhovskii.ipynb` and

`Si220_17p45keVScrewDislChukhovskii.yaml` for the screw dislocation,

and

`SingleRealization_60degDislocationSi220_17p45keVChukhovskii.ipynb` and

`Si220_17p45keVDislChukhovskii.yaml` for the 60-degree mixed dislocation.

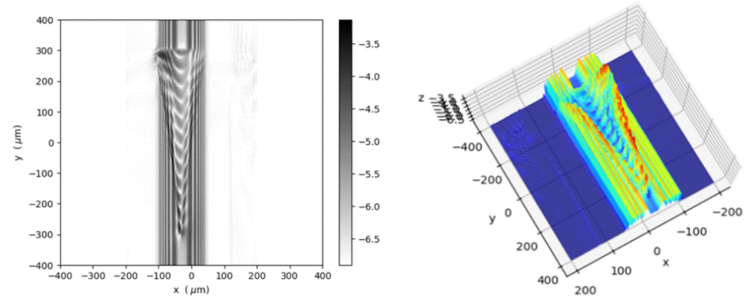

Figure 11. Simulation of a topography of a 60 deg dislocation in a Si crystal by the Lang method for (440) reflection. The intensity scale is logarithmic

7. SUMMARY

We have demonstrated that the Fast Fourier Transform Beam Propagation Method (FFT BPM) can be applied to simulate dynamic diffraction effects across a wide range of problems, including scattering from deformed crystals of any shape in Bragg, Laue, or asymmetric geometries. We successfully reproduced results simulated using the Takagi–Taupin equations[17] and presented in the literature for bent crystals and dislocations.

FFT BPM is well suited to simulate with a wide spectral range for non-Gaussian (e.g FEL SASE beams). beams including numerical code is very compact ...

1. Compact code Python - easy implementation, can be easily shared with x-ray comunity via github

2. Can be implemented naturally at multicore machine where single realization reflection object can be computed in parallel to other reflections having different parameters e.g. photon energy, incidence angle, etc. Thus, the calculation of rocking curves or time-dependent diffraction can be implemented as an embarrassingly parallel problem.

ACKNOWLEDGMENTS

This work was supported by the U.S. Department of Energy (DOE) Contract No. DE-AC02-76SF00515 with SLAC.

REFERENCES

[1] Krzywinski, J. and Halavanau, A., "Time-dependent dynamical Bragg diffraction in deformed crystals by the beam propagation method," *Acta Crystallographica Section A* **78**, 465–472 (Nov 2022).

[2] Krzywinski, J. and Halavanau, A., "Crystal-fft-bpm," *Python code on github* (2022).

[3] Hadley, G. R., "Wide-angle beam propagation using padé approximant operators," *Opt. Lett.* **17**(20), 1426–1428 (1992).

[4] Ersoy, O. K., [*Diffraction, Fourier Optics and Imaging*], John Wiley I& Sons, Ltd (2007).

[5] Gaudin, J., Ozkan, C., Chalupský, J., Bajt, S., Burian, T., Vyšín, L., Coppola, N., Farahani, S. D., Chapman, H. N., Galasso, G., Hájková, V., Harmand, M., Juha, L., Jurek, M., Loch, R. A., Möller, S., Nagasono, M., Störmer, M., Sinn, H., Saksl, K., Sobierajski, R., Schulz, J., Sovak, P., Toleikis, S., Tiedtke, K., Tschentscher, T., and Krzywinski, J., "Investigating the interaction of x-ray free electron laser radiation with grating structure," *Opt. Lett.* **37**(15), 3033–3035 (2012).

[6] Andrejczuk, A., Krzywinski, J., and Bajt, S., "Influence of imperfections in a wedged multilayer laue lens for the focusing of x-rays investigated by beam propagation method," *Nuclear Instruments and Methods in Physics Research Section B: Beam Interactions with Materials and Atoms* **364**, 60 – 64 (2015).

[7] Morgan, A. J., Prasciolu, M., Andrejczuk, A., Krzywinski, J., Meents, A., Pennicard, D., Graafsma, H., Barty, A., Bean, R. J., Barthelmess, M., Oberthuer, D., Yefanov, O., Aquila, A., Chapman, H. N., and Bajt, S., "High numerical aperture multilayer laue lenses," *Scientific Reports* **5**(1), 9892 (2015).

[8] Bajt, S., Prasciolu, M., Morgan, A. J., Chapman, H. N., Krzywinski, J., and Andrejczuk, A., "One dimensional focusing with high numerical aperture multilayer laue lens," *AIP Conference Proceedings* **1696**(1), 020049 (2016).

[9] Authier, A., [*Dynamical Theory of X-Ray Diffraction*], International Union of Crystallography Monographs on Crystallography, Oxford University Press, Oxford (2003).

[10] Omelyan, I., Mryglod, I., and Folk, R., "Optimized forest–ruth- and suzuki-like algorithms for integration of motion in many-body systems," *Computer Physics Communications* **146**(2), 188–202 (2002).

[11] del Rio, M. S. and Dejus, R. J., "Xop v2.4: recent developments of the x-ray optics software toolkit," *Proc.SPIE* **8141**, 8141 – 8141 – 5 (2011).

[12] Zhu, D., Cammarata, M., Feldkamp, J. M., Fritz, D. M., Hastings, J. B., Lee, S., Lemke, H. T., Robert, A., Turner, J. L., and Feng, Y., "A single-shot transmissive spectrometer for hard x-ray free electron lasers," *Applied Physics Letters* **101**, 034103 (07 2012).

[13] Kujala, N., Freund, W., Liu, J., Koch, A., Falk, T., Planas, M., Dietrich, F., Laksman, J., Maltezopoulos, T., Risch, J., Dall'Antonia, F., and Grünert, J., "Hard x-ray single-shot spectrometer at the European X-ray Free-Electron Laser," *Review of Scientific Instruments* **91**, 103101 (10 2020).

[14] Samoylova, L., Boesenberg, U., Chumakov, A., Kaganer, V., Petrov, I., Roth, T., Rüffer, R., Sinn, H., Terentyev, S., and Madsen, A., "Diffraction properties of a strongly bent diamond crystal used as a dispersive spectrometer for XFEL pulses," *Journal of Synchrotron Radiation* **26**, 1069–1072 (Jul 2019).

[15] Besedin, I. S., Chukhovskii, F. N., and Asadchikov, V. E., "Study of the diffraction contrast of dislocations in x-ray topo-tomography: A computer simulation and image analysis," *Crystallography Reports* **59**, 323–330 (May 2014).

[16] Kowalski, G. and Gronkowski, J., "On the intermediary image in x-ray section topography," *physica status solidi (a)* **71**(2), 611–617 (1982).

[17] Scalora, M. and Crenshaw, M. E., "A beam propagation method that handles reflections," *Optics Communications* **108**(4), 191 – 196 (1994).